

13.2 IMPACT OF CONFIGURATIONS OF RAPID INTERMITTENT ASSIMILATION OF WSR-88D RADAR DATA FOR THE 8 MAY 2003 OKLAHOMA CITY TORNADIC THUNDERSTORM CASE

Ming Hu and Ming Xue*

Center for Analysis and Prediction of Storms and School of Meteorology
University of Oklahoma, Norman, Oklahoma

1. INTRODUCTION

The operational WSR-88D Doppler radar network of the United States (Crum and Alberty 1993) has dramatically improved the ability of severe weather warning in routine operations (Serafin and Wilson 2000); it is also playing an important role in storm-scale data assimilation and model initialization, because it is the only observational network that can resolve convective storms. However, the analysis of radar data to arrive at a complete set of initial conditions for a numerical weather prediction (NWP) model is challenging, because radars only observe a very limited set of parameters, mainly, the radial velocity and reflectivity. Further, their spatial coverage is usually incomplete. To build up suitable dynamically balanced storms in a model from radar observations, retrieval or assimilation methods that take advantage of the high data frequency is usually necessary.

Four-dimensional variational (4DVAR) data assimilation method is considered ideal for this purpose and some encouraging results with both simulated and real radar data have been obtained (Sun *et al.* 1991; Sun and Crook 1997,1998). However, the difficulty of getting the adjoint code and the high cost of computation are limiting its use in research and operation. Another relatively new technique is the ensemble Kalman filter (EnKF) data assimilation, which can produce the similar quality assimilation of thunderstorms with single-Doppler radar data as the 4DVAR (Snyder and Zhang 2003; Zhang *et al.* 2004; Tong and Xue 2005). While also expensive in computation, EnKF method is easier to implement and more flexible.

Other simpler and faster methods to build up balanced storms in analysis are retrieving unobserved wind components (Qiu and Xu 1992; Qiu and Xu 1994; Xu *et al.* 1994; Shapiro *et al.* 1995; Gao *et al.* 2001) and then thermodynamic fields from wind fields (Gal-Chen 1978). The retrieved fields can then be analyzed into mode initial conditions to initialize a model (Weygandt *et al.* 2002a; 2002b). The quality of retrieved thermodynamic fields heavily depends on the quality of the wind retrievals and the frequency of the wind fields.

Another efficient way to assimilate multiple radar volume scans is intermittent assimilation cycles with fast analysis method, such as three dimensional variational (3DVAR) analysis, ARPS (Xue *et al.* 1995; 2000; 2001) Data Analysis System (ADAS, Brewster 1996) and complex cloud analysis of the ARPS. The ARPS 3DVAR (Gao *et al.* 2002; 2004) can analyze the radar radial velocity data and other conventional data variationally, while the ADAS uses Bratseth (1986) scheme to analyze conventional observations and a simple procedure to adjust wind from radial velocity. The cloud analysis procedure retrieves thermodynamic and microphysical fields from the reflectivity according to semi-empirical rules (Zhang *et al.* 1998; Zhang 1999) and can be used with both the ARPS 3DVAR and ADAS.

Recently, Hu *et al.* (2005a; 2005b) demonstrated for a tornado thunderstorm case that occurred on 28 March 2000 in downtown Fort Worth, Texas, that the ARPS 3DVAR and the ARPS cloud analysis together, through 1-hour-long intermittent assimilation cycles at 10 minute intervals, are able to successfully build up reasonably balanced storms in the model. Starting from such an initial condition, the ARPS model is able to predict individual storm cells with reasonable accuracy for up to two hours. The prediction captured the supercell characteristics of the storm that spawned two individual tornadoes. An in-cloud temperature adjustment scheme based on the moist-adiabat associated with a lifted low-level parcel is used in their control experiment.

In this study, the above assimilation and forecast system is applied to the 8 May 2003

* Corresponding Author Address: Dr. Ming Xue, School of Meteorology, University of Oklahoma, 100 East Boyd, Norman, OK 73019, USA. E-mail: mxue@ou.edu

Oklahoma City tornadic thunderstorm case, which will be referred to as the OKC case in this paper. Data from the Oklahoma City WSR-88D radar (KTLX) are assimilated. Again using a nested grid at 3 km horizontal resolution, the ARPS model is able to predict the propagation and supercell characteristics of the OKC storm accurately for up to 2.5 hours. It is found, however, that the results of assimilation and prediction are sensitive to the details of the assimilation configurations. The assimilation frequency, the in-cloud temperature adjustment scheme used and the length and coverage of assimilation window (AW) all affect the results. It is the goal of this study to investigate how these different configurations affect the results and why. In addition, this study serves to document the application of our 3DVAR and cloud analysis procedure to another tornadic supercell case. This case differs from the Fort Worth case in that the thunderstorms were more isolated and lasted for a longer period of time.

The organization of this paper is as follows. In section 2, the 8 May Oklahoma City tornadic thunderstorm case is introduced. In section 3, we introduce the design of a set of experiments for studying the impact of the assimilation configurations. A detailed comparison among experiments is presented in section 4 and the results are further discussed in section 5. Section 6 provides a brief summary of the key findings.

2. THE 8 MAY 2003 OKLAHOMA CITY TORNADIC THUNDERSTORM CASE

At about 2210 UTC (1610 Local Standard Time or LST) on 8 May 2003, Moore, a suburb city about 15 km south of the Oklahoma City (OKC thereafter), Oklahoma, was struck by a major tornado for the 4th time in 5 years. The tornado tracked east-northeast for about 30 km on the ground, from Moore to Choctaw, and dissipated at 2238 UTC (Fig. 1, all times will be in UTC unless otherwise noted). It caused large areas of F3 (on Fujita scale of tornado intensity) and small areas of F4 damages south and east of OKC, and many F2 damages in the Moore area. This tornado produced \$370 million worth of damages and more than 100 injuries, but fortunately no death. It is named the OKC tornado by National Weather Service as it struck the general OKC area. The parental storm is referred as the OKC tornadic thunderstorm.

Two additional short-lived tornadoes from the same storm were reported near Moore. The first briefly tornado occurred at 2200. The second F0 tornado began at 2204 and stayed on the ground

along WSW (west-southwest) to ENE (east-northeast) path for nearly 3 km but dissipated just before the OKC tornado outbreak.

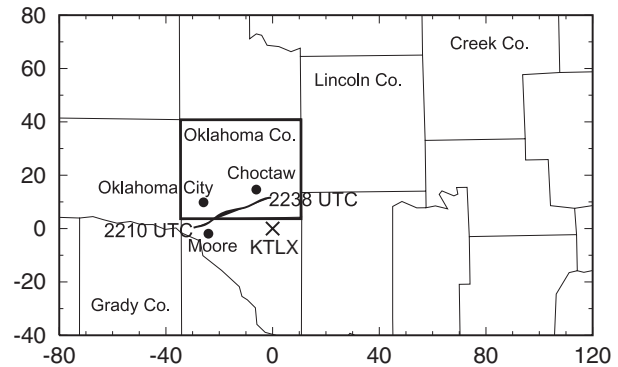


Fig. 1. Map of counties and cities related to the 8 May 2003 OKC tornadic thunderstorm. The dark line segment starting at 2210 northwest of Moore and ending at 2238 south Choctaw marks the rough path of the OKC tornado. The x and y distances are in kilometer and are relative to the KTLX radar marked by \times in the figure. The Oklahoma County is highlighted.

On 8 May 2003, the synoptic-scale environment over Oklahoma was favorable for tornadic thunderstorms. A surface low formed in the early morning in southeast Colorado and propagated northeastwards across Kansas during the daytime. The Oklahoma and Texas had been exposed to southerly flows for all day and a north-south oriented dryline formed over western Texas and the Texas-Oklahoma panhandle area by 1200 (0006 LST). The dryline then moved eastwards into western Oklahoma and by 1800 (1200 LST) it was located about 200 km west of OKC. During the daytime, the upper level flows over the Oklahoma were mainly southwesterlies with the wind speed slightly increasing before the thunderstorms.

The 1800 Norman, Oklahoma (OUN) sounding shows a moderate to large instability with a 2453 J kg^{-1} CAPE and a 57 J kg^{-1} CIN. The vertical shear of horizontal winds over the lowest 6 km is about 20 m s^{-1} . Both instability and shear suggest a strong potential for supercell and tornado.

At 2040, the OKC tornadic thunderstorm was initiated east of the dryline, as a weak echo observed by Oklahoma City (KTLX) radar. The evolution of the storm is displayed by a series of low-level reflectivity regions whose values are greater than 35 dBZ (Fig. 2). The storm developed

into a strong cell by 2101 and was located at (-75, -50) km relative to KTLX radar. It then propagated northeastwards and grew significantly in size in the next hour. At 2201, a pronounced hook appendage structure is found at the southwestern end of the storm, northwest of Moore, indicating the presence of a tornado or mesocyclone. The supercell storm propagated east-northeastwards, and then became weaker from 2300, 8 May and dissipated by 0020, 9 May. In addition to the OKC

storm, three other storms are also shown in Fig. 2 and are referred to storms A, B, and C. Storm A was initiated a little earlier than the OKC storm east of the dryline but dissipated by 2130. Storm B was initiated later than the OKC storm and lasted for only about one hour. Storm C was split from the OKC storm and dissipated quickly during its leftward propagation.

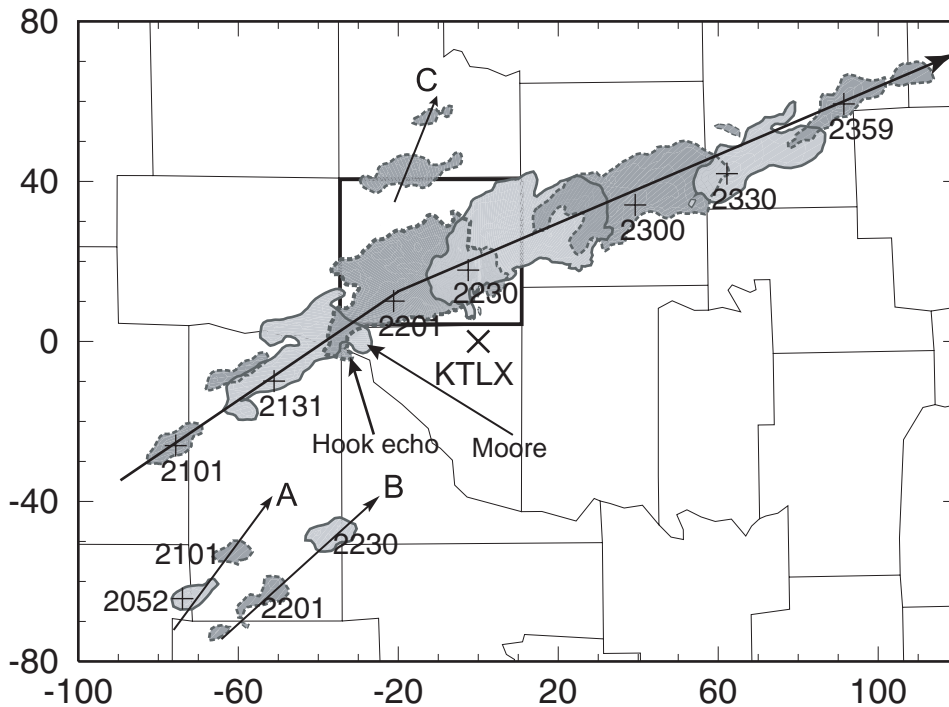


Fig. 2. Regions of radar echoes exceeding 35 dBZ as observed by KTLX radar at the 1.45° elevation. The echoes are at 30-minute intervals from 2101 to 2359, of 8 May 2003. The grayscales of the echoes at two consecutive times are different, so are their outlines. The locations of the maximum reflectivity are marked by + signs, together with the corresponding times. The x and y coordinates are in kilometers and have their origin at the KTLX radar site that is marked by x. The arrow lines are the trajectories of the OKC storm and the storms A, B, and C. Also, the look echo at 2201 and Moore are pointed by arrows. The Oklahoma County is highlighted.

3. DESIGN OF ASSIMILATION AND FORECAST EXPERIMENTS

In this paper, data from KTLX radar are assimilated to study the impact of different assimilation configurations on the initialization and prediction of the OKC storm. The low-level reflectivity observations from the same radar are used to evaluate the quality of the forecasts, which

are the only available observations having enough temporal and spatial resolutions for resolving the storm.

For all experiments, two one-way nested grids, with 9 and 3-km horizontal resolutions, respectively, are used. The 9-km grid covers an area of 2300x2300 km² with Oklahoma located roughly at the center. The 3-km grid is 580x580 km² in size and covers the entire state of Oklahoma and parts of Texas and Kansas. Both 9-

km and 3-km simulations use the same vertical grid that stretches from about 20 m at the surface to 770 m at the model top that is located at 21.1 km height. The ARPS model with full physics is used during the assimilation and in the forecast. The ARPS 3DVAR is used to analyze conventional and radial velocity data, while the cloud analysis procedure is used to adjust in-cloud temperature, moisture and hydrometers fields using reflectivity data.

Only one 9-km simulation is conducted and its forecast results provide the background for the first 3-km analysis, and the boundary conditions for 3-km assimilation and forecast. The 9-km simulation includes 1-hour assimilation cycles over a 6 hour period from 1800, 8 May to 0000, 9 May. The 9-km analysis uses the NCEP Eta model 1800 analysis as the background. Only rawinsonde and wind profiler data are used in the analyses. The lateral boundaries are forced by the Eta 1800 forecasts at 3-hour intervals.

The 3-km control experiment starts at 2030, slightly earlier than the initiation time of the OKC storm. The one-hour long assimilation cycles with 10-minute intervals cover the entire initiation stage of the storm. Both reflectivity and radar velocity data are assimilated along with the upper air data when available. The two-pass strategy with different characteristic spatial scale for each pass is used in the 3DVAR. The upper-air data are analyzed in the first pass using a horizontal scale length of 120 km and the radial velocity data are analyzed in the second pass using a scale length of 6 km. For the 3-km control experiment, a 2.5-hour forecast is conducted from the end result of assimilation at 2130, 40 minutes before the OKC tornado outbreak northwest of Moore.

Based on the control experiment, a series of other 3-km experiments are conducted, using different assimilation configurations, to study their impacts on the assimilation and subsequent forecast. The configuration parameters that are varied include assimilation frequencies (or intervals), in-cloud temperature adjustment schemes, and the lengths and coverages of AW.

A total of fifteen 3-km experiments (Table 1) are conducted, including the control. These experiments can be classified into two groups according to assimilation frequency, experiments with 5-minute and 10-minute intervals. In each group, the length of the AW varies from 30 to 60 minutes and the AW covers different stages of the OKC storm development. The latter include the entire initiation stage (from 2030 to 2130), the early stage of initiation (from 2030 to 2110 or 2120), and the late stage of initiation (from 2040,

2050 or 2060 to 2130). For in-cloud temperature adjustment, two schemes are available in the ARPS cloud analysis package. One is based on the latent heat release (Zhang *et al.* 1998, referred to as LH scheme) associated with cloud condensate amount, and the other is based on a moist adiabatic temperature profile (Brewster 2002, referred to as MA scheme). All experiments with 5-minute intervals use the MA scheme except for experiments 5B30E30LH and 5B60E30LH, which use the LH scheme. All experiments with 10-minute analysis intervals use the LH scheme except for experiment 10B30E30MA which uses the alternative method. The details of the two temperature adjustment schemes and the ideal combination of one of them with other configuration parameters are discussed in next section.

4. THE RESULTS OF ASSIMILATION AND FORECAST EXPERIMENTS

In this section, we first discuss the results of control experiment 10B30E30LH (also called CNTL) which produced the best OKC storm forecast among the 15 experiments. The experiments with different assimilation frequencies, in-cloud temperature adjustment schemes, and assimilation lengths and coverage are then discussed and compared. Finally, the results of experiment 5B60E30LH are discussed as an example of applying the above conclusions of assimilation configurations to improve the forecast.

4.1. The Experiment with the Best Forecast

The experiment that produces the best forecast, i.e., control experiment 10B30E30LH, employs a 1-hour-long AW from 2030 to 2130 with 10-minute analysis cycles (about every other radar volume scan). The LH scheme is used for in-cloud temperature adjustment (Table 1). As mentioned before, the first echo of the OKC storm appeared at 2040 and the first tornado from the storm occurred at 2200. The AW of this experiment, therefore, covers the entire initial development stage of the storm and the final analysis has a half-hour lead time from the first tornado.

The regions with reflectivity exceeding 45 dBZ, as observed by the OKC KTLX radar at the 1.45° elevation, are shown in Fig. 3 together with the corresponding predicted reflectivity fields from 10B30E30LH. The time period shown in Fig. 3 is from 2130, 8 May to 0000, 9 May 2003. The observed storm first appeared at the northeast corner of Grady County (c.f., Fig. 1), propagated

east-northeastwards through Oklahoma and Lincoln Counties, and arrived at east-central Creek County 2.5 hours later (Fig. 3a). Experiment 10B30E30LH predicts the observed storm motion accurately (Fig. 3b); the predicted storm moves in essentially the same direction and at about the same speed as the observed storm. The location errors of the maximum reflectivity of the predicted OKC storm are within 8 km in the entire 2.5 hours of forecast. The observed storm grew quickly from 2131 to 2201, remaining a supercell with a large area of strong reflectivity exceeding 45 dBZ (shown as shaded regions in Fig. 3). Pronounced hook echo existed at the southwest end of the high-reflectivity region between 2201 and 2300. After 2300, the storm weakened, and by 2359 only a small area of high reflectivity (>45 dBZ) remained. The main characteristics of the observed storm are captured by the forecast; the predicted storm reaches its maximum intensity at about 2200, but remains a strong supercell until the end of forecast at 0000. Overall, 10B30E30LH successfully predicts the development and propagation of the OKC thunderstorm even though it is somewhat too strong in the last hour of the real storm.

The model-predicted reflectivity fields at 1.45° elevation at 2200 and 2300 from 10B30E30LH are shown in more detail in Fig. 4 (right column),

together with the corresponding observations (left column). At 2200, the time of the first tornado outbreak, a clear hook echo is seen at the southwest end of the observed storm (Fig. 4a) and two small left-moving cells are seen north of the storm. The half-hour forecast of 10B30E30LH at this time produces the right position and strength of the storm, but does not exhibit a clear hook shape at the SW end (Fig. 4b). The predicted storm system also exhibits a sign of splitting at this time, but the left-moving cell is located to the NE instead of north of the main cell and is stronger than the observed ones. One hour later, the observed storm remained strong and moved to central Lincoln County (Fig. 4c). Although the OKC tornado ended about 20 minutes earlier, the storm still possesses strong reflectivity gradient and hook-shaped echo at its south flank, indicating its supercell characteristics. Again, the 1.5 hour forecast of 10B30E30LH at 2300 gives accurate position and strength of the storm (Fig. 4d); as observed, the predicted storm also exhibits supercell characteristics, a hook-shaped echo with strong reflectivity gradient at its south flank. The mid-level flows also show strong rotation in the model (not shown). Therefore, many details of the observed storm are captured well by the prediction in control experiment 10B30E30LH.

Table 1. Assimilation configurations of 3-km experiments

Name*	Interval (minutes)	Length (minutes)	Coverage (UTC)	In-cloud temperature adjustment
10B30E30LH (CNTL)	10	60	2030–2130	LH
10B30E30MA	10	60	2030–2130	MA
10B30E20	10	50	2030–2120	LH
10B30E10	10	50	2030–2110	LH
10B40E30	10	50	2040–2130	LH
10B50E30	10	40	2050–2130	LH
10B60E30	10	30	2060–2130	LH
5B30E30MA	5	60	2030–2130	MA
5B30E30LH	5	60	2030–2130	LH
5B30E20	5	50	2030–2120	MA
5B30E10	5	40	2030–2110	MA
5B40E30	5	50	2040–2130	MA
5B50E30	5	40	2050–2130	MA
5B60E30	5	30	2100–2130	MA
5B60E30LH	5	30	2100–2130	LH

* Characters B and E followed by a number denote, respectively, the beginning and ending time of the assimilation window in minutes.

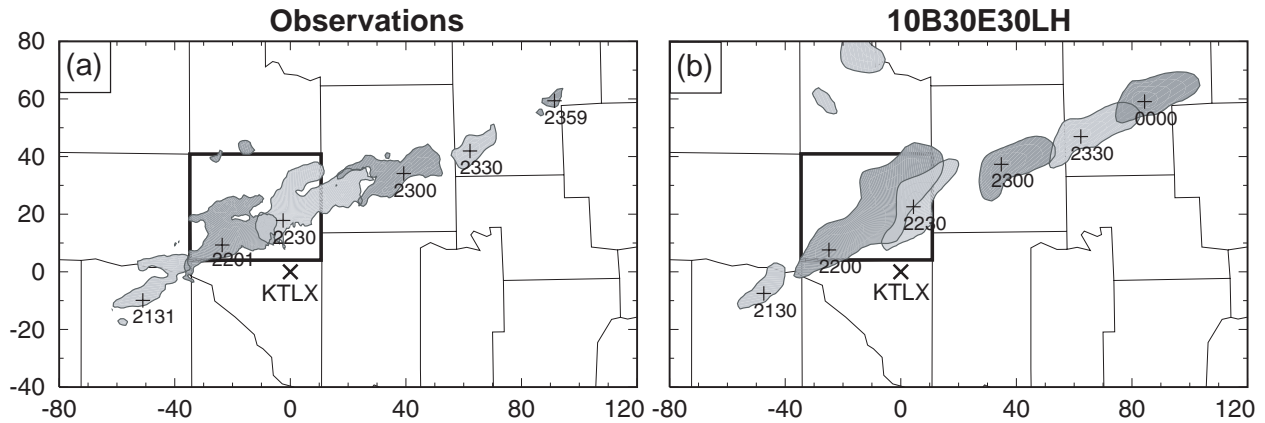


Fig. 3. As in Fig. 2, but for (a) 2130, 8 May to 0000, 9 May 2003, at 30 minute intervals, and (b) the corresponding predicted fields from experiment 10B30E30LH. Regions with reflectivity exceeding 45 dBZ are shown. The locations of the maximum reflectivity of the OKC storm are marked by + signs together with the corresponding times. The domain shown represents the portion of the 3-km grid between 210 and 410 km in east-west direction and from 260 to 380 km in north-south direction.

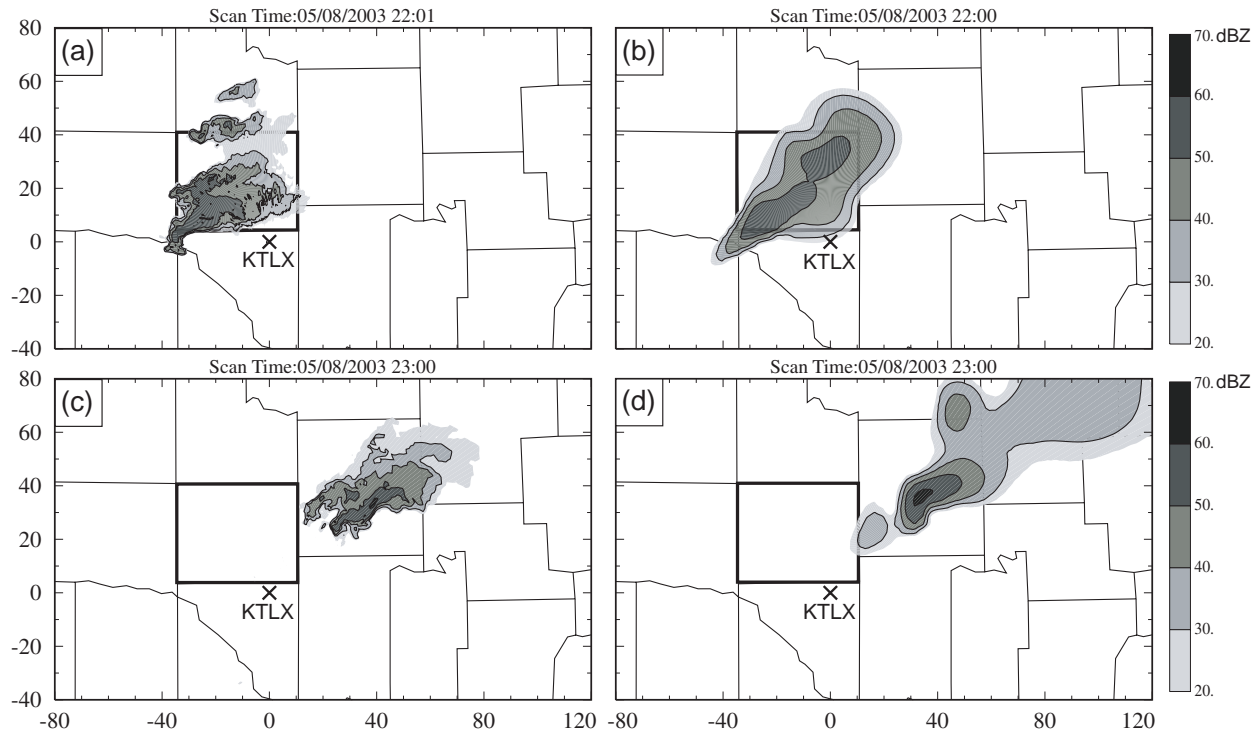


Fig. 4. Observed reflectivity fields at the 1.45° elevation of the KTLX radar (left column), and the corresponding predicted reflectivity from the experiment 10B30E30LH (right column), at 2200 and 2300, 8 May 2003. The reflectivity contours are at 30, 40, 50, and 60 dBZ. The domain shown is the same as Fig. 3.

4.2. The Impact of the Frequency of Analysis Cycles

In the control experiment, the KTLX radar data are used every 10 minutes, while the volume scan frequency of operational WSR-88D Doppler radars (such as KTLX) in precipitation mode is about 5 minutes. To study the impact of the frequency of analysis cycles on the prediction of storms, experiment 5B30E30MA is conducted. This experiment is the same as the control except for its 5-minute analysis cycles and the use of MA scheme for in-cloud temperature adjustment (Table 1). The reason of using a different in-cloud temperature adjustment scheme is discussed in next subsection.

The regions with predicted reflectivity exceeding 45 dBZ at the 1.45° elevation from experiment 5B30E30MA are shown in Fig. 5, at every 30 minutes. Compared with the observations (Fig. 3a), 5B30E30MA predicts the motion of the OKC storm very well, but gives a wrong trend of storm evolution. Contrary to the observations, the predicted storm becomes weaker from 2200 to 2300 and then stronger from 2300 on. The positions of the predicted maximum reflectivity in 10B30E30LH are better than those of 5B30E30MA in most of the times (Fig. 3b, Fig. 5) and the evolution of storm strength is better captured by 10B30E30LH too, even though 10B30E30LH over-predicts the intensity of the storm at the dissipation stage.

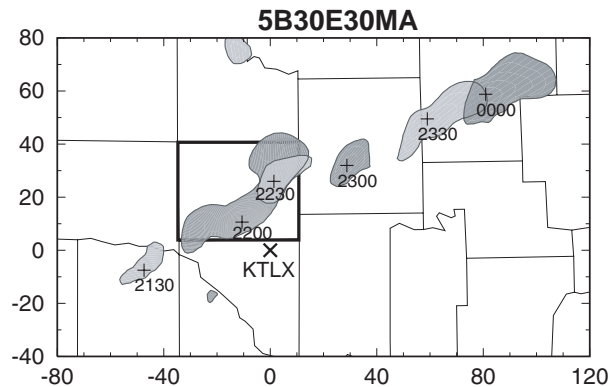


Fig. 5. As Fig. 3b, but for experiment 5B30E30MA.

To quantitatively compare the quality of the forecasts from 10B30E30LH and 5B30E30MA, equitable threat scores (ETS, Schaefer 1990) of the predicted reflectivity at the 1.45° elevation for the 45 dBZ threshold are calculated against the observations and plotted in Fig. 6. The ETS is

originally designed for large scale precipitation prediction and should be applied with caution for small-scale convection systems. ETS was used in a similar way as we do here in Hu et al. (2005b). Fig. 6 shows that the first-hour forecasts (from 2130 to 2230, 8 May) of the two experiments are similar except for 0.75 hour when 5B30E30MA is better. For the next 1.5 hours, 10B30E30LH has much higher scores than 5B30E30MA. The largest difference occurs at 1.5 hours (2300), when the scores for 10B30E30LH and 5B30E30MA are 0.48 and 0.29, respectively. This is the time when the storm in 5B30E30MA is too weak (Fig. 5). The comparisons of equitable threat scores of these two experiments agree with the earlier subjective evaluation.

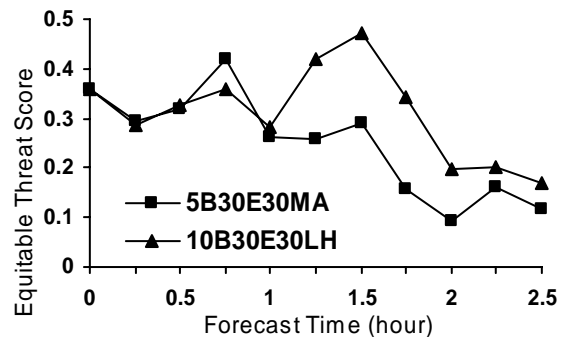


Fig. 6. Equitable threat scores for the predicted 1.45° elevation reflectivity for 45 dBZ threshold, for experiments 5B30E30MA and 10B30E30LH.

Usually, the data assimilation tries to use all available observations to obtain the best possible observations for forecast, but both subjective evaluation and ETS for the previous two experiments suggest that the experiment with lower assimilation frequency (10 minute intervals) gives a better forecast. The reason is complex and appears to be related to both the ability of the analysis procedure to generate balanced storms in the initial fields and the ability of the model in establishing a suitable balance among different variables through adjustment. In our experiment, the radial velocity data are analyzed by the ARPS 3DVAR under a mass divergence constraint and the reflectivity data are used through the cloud analysis to adjust in-cloud temperature, moist, and hydrometer fields. Apart from the velocity components that are coupled through the mass continuity equation, the other analysis variables are analyzed more or less independently. Therefore, the analysis fields are not in balanced

in general or consistent with model dynamics and physics. Starting from such initial conditions, the model forecast must undergo some adjustments during the initial period to build up a balanced storm and such adjustments take some time to complete. For this reason, it is desirable that we start a new analysis after the model state reaches a reasonable balance through model adjustment; too short analysis cycles do not necessarily lead to better final analysis. This is in general not true for more sophisticated data assimilation techniques such as the ensemble Kalman filter method, in which flow-dependent background error covariances help produce balanced analysis that allows for high frequency analysis cycles without degrading the final analysis. Xue et al. (2005) show with simulated data, that radar data at 1-minute volume scan intervals produce better analysis than those collected at lower volume scan frequencies.

The maximum vertical velocity (W_{max}) can be used as an indicator of the initial adjustment during the model forecast. The maximum vertical velocities of the first 20 minutes of model forecasts starting from the analyses around 0 (2030, 2035, initial stage), 30 (2100, 2105, middle stage), and 50 (2120, 2125, late stage) minutes into the AW are plotted in Fig. 7 for experiments 5B30E30MA and 10B30E30LH. The curves of W_{max} at all three stages show similar shapes in both experiments (Fig. 7). For the forecasts starting from the first analysis, over the period from 0 to 20 minutes, W_{max} increases from values below 5 m s^{-1} to maximum values above 33 m s^{-1} in 12 to 14 minutes and then drop sharply in the next 6 to 8 minutes. For the forecasts starting at 30 minutes, W_{max} values increase from analyzed values between 20 and 25 m s^{-1} to their maximum values close to 40 m s^{-1} in 5 to 7 minutes and then drop more slowly. For the forecasts starting at 50 minutes, W_{max} values increase sharply in the first 1 to 2 minutes, reach the maximum values slowly in 7 to 8 minutes, and then decrease slowly. It is clear that even for the forecasts that start from cycled initial conditions, such as those at 30 and 50 minutes, the model still needs more than 5 minutes to establish strong vertical motion and in the process producing a more balanced state. When analysis cycles shorter than 10 minutes are used, the model does not have enough time to spin up the updraft in the model, from the new analysis whose updraft strength tends to be reduced by the analysis step. The latter is shown by dash lines in Fig. 7a as the W_{max} values at 5, 35 and 55 minutes are clearly lower than the values from the forecasts starting 5 minutes earlier.

For this reason, 10-minute analysis cycles work better than 5-minute cycles. On the other hand, when the analysis intervals are too long, such as 15 minutes, the insufficiently spun up storms in the model would have weakened significantly by the time of next analysis. This explains why the 10-minute analysis cycles work better than 5 minute cycles.

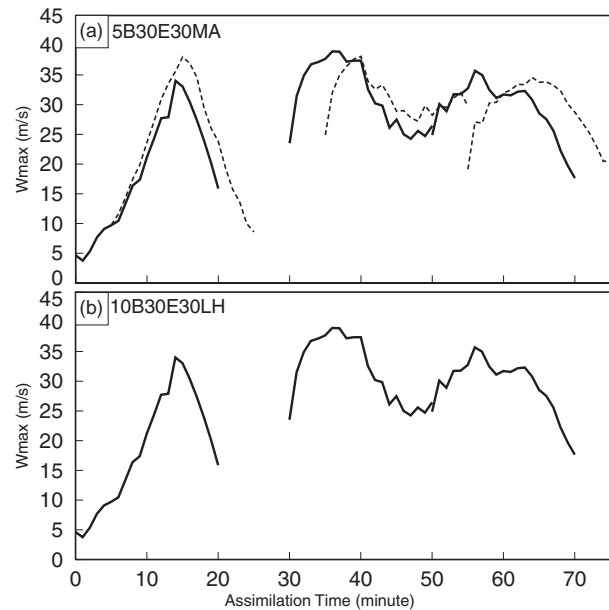


Fig. 7. The maximum vertical velocities for the first 20 minutes of forecasts starting from analyses at 0 (2030), 30 (2100), and 50 (2120) minutes into the assimilation cycles (solid lines) and from the analyses following the above analyses (dash lines), for experiments 5B30E30MA (a) and 10B30E30LH (b).

4.3. The Impact of In-cloud Temperature Adjustment Schemes

As mentioned earlier, the ARPS cloud analysis has two in-cloud temperature adjustment schemes: the latent heat scheme (LH) that calculates the temperature adjustment from the latent heat release corresponding to the added cloud water and ice by the analysis, and the moist-adiabat (MA) scheme that adjusts in-cloud temperature based on a moist adiabat corresponding to an air parcel lifted from the low-level. The effect of entrainment is considered for the latter scheme. The MA scheme is more consistent with the physics of a convective storm because it reflects the temperature change in an ascending moist air

parcel while repeated applications of the first scheme can lead to multiply counting the same latent heating associated with the condensed water or ice.

The temperature adjustment is very important for sustaining existing convection and the use of different schemes can impact the storm forecast significantly (Hu *et al.* 2005b). To further study the impact of the temperature adjustment schemes and their interaction with the other assimilation parameters, experiments 10B30E30MA and 5B30E30LH are conducted. They are same as 10B30E30LH and 5B30E30MA, respectively, except for the temperature adjustment scheme used (Table 1). The regions of predicted reflectivity exceeding 45 dBZ, at the 1.45° elevation, are shown in Fig. 8 for 10B30E30MA and 5B30E30LH. The ETS of the same reflectivity fields, for the 45 dBZ threshold, are plotted in Fig. 9. The scores from 5B30E30MA are also included for the convenience of comparison.

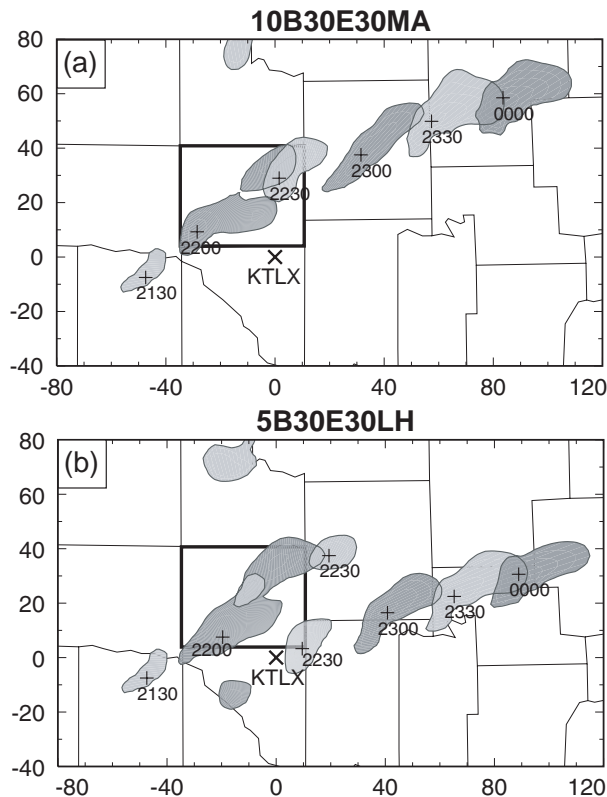


Fig. 8. Same as Fig. 3b, but for experiments 10B30E30MA (a) and 5B30E30LH (b).

Similar to 5B30E30MA, 10B30E30MA predicts the propagation of the OKC storm well but the predicted change in the storm strength is opposite to the observed change (Fig. 8a and Fig. 5).

Compared to 10B30E30LH, the predicted storm in 5B30E30LH dissipates too early. This early dissipation appears to be related to the spurious cell that develops in the model south of the OKC storm and propagates east-northeastward during the last two hours of forecast (Fig. 8b and Fig. 3b).

The ETSs of these four experiments agree with the subjective evaluation (Fig. 9 and Fig. 6). 10B30E30LH has the highest scores most of the times, especially for forecasts over 1 hour; 10B30E30MA has lower scores than 5B30E30MA most of the times because the former over-predicts the OKC storm even more at those times; 5B30E30LH has zero scores after 1 hour because the predicted OKC storm dissipates in 1 hour forecast.

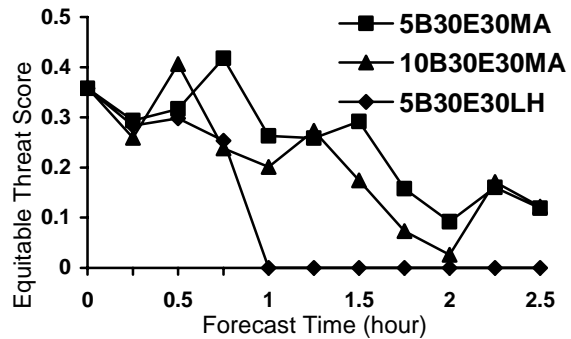


Fig. 9. Equitable threat scores of predicted reflectivity for the 45 dBZ threshold for experiments 5B30E30MA, 5B30E30LH, and 10B30E30MA.

The in-cloud temperature adjustment increases the temperature inside the storm therefore increases potential energy (or buoyancy) in the system that supports the development of the storm. To quantitatively estimate the effect of temperature adjustment by two different schemes, the total potential energy added to the model atmosphere by the temperature adjustment in all analysis cycles is calculated for the above four experiments and the results are 9.54×10^{16} , 16.79×10^{16} , 2.35×10^{16} and 4.16×10^{16} J in 10B30E30LH, 5B30E30LH, 10B30E30MA and 5B30E30MA, respectively. The LH scheme adds much more, or approximately 4 times as much potential energy than the MA scheme for the assimilations with the same number of cycles. Further, the use of more cycles tends add more energy into the system and it is more so with the LH scheme by design.

As an important indicator of the vigor of a storm, the vertical velocity fields at 7 km MSL are shown in Fig. 10 for 10B30E30LH, 5B30E30MA, 10B30E30MA, and 5B30E30LH. Two updraft centers, one related to the OKC storm and the other related to storm A (c.f., Fig. 2), are found at the end of the assimilation in all four experiments. However, their strengths are very different, because of the use of the different temperature adjustment schemes and analysis frequencies (Fig. 10). With a higher analysis frequency (5 minute interval) and the LH scheme, the assimilation of 5B30E30LH produces the strongest updraft of the OKC storm (Fig. 1d) among all four experiments, but the predicted OKC storm dissipates in about one hour (Fig. 8b). At the same time, storm A, shown as the southern updraft, develops into a strong storm in the forecast instead dissipating as observed. The wrong behaviors of both OKC storm and storm A and the extra strength of the

updrafts indicate that too much potential energy (16.79×10^{16} J) had been added into both storms. The over-loaded energy causes the too fast development and too earlier dissipation of the OKC storm, and causes the spurious intensification of storm A. The dissipation of OKC storm might be caused by the blowing of low-level inflow in the storm by storm A. At the opposite end, using a lower frequency (10 minute interval) and the MA scheme, 10B30E30MA adds only about 1/8 of the potential energy as 5B30E30LH and the resulting updrafts are much weaker and smaller in size (Fig. 10c). Although storm A correctly dissipates quickly in the forecast, the predicted OKC storm strengths very slowly in the entire 2.5 hours of forecast (Fig. 8a), indicating that too little potential energy has been added into the OKC storm. This slows the development of the OKC storm and delays the predicted storm entering dissipation stage.

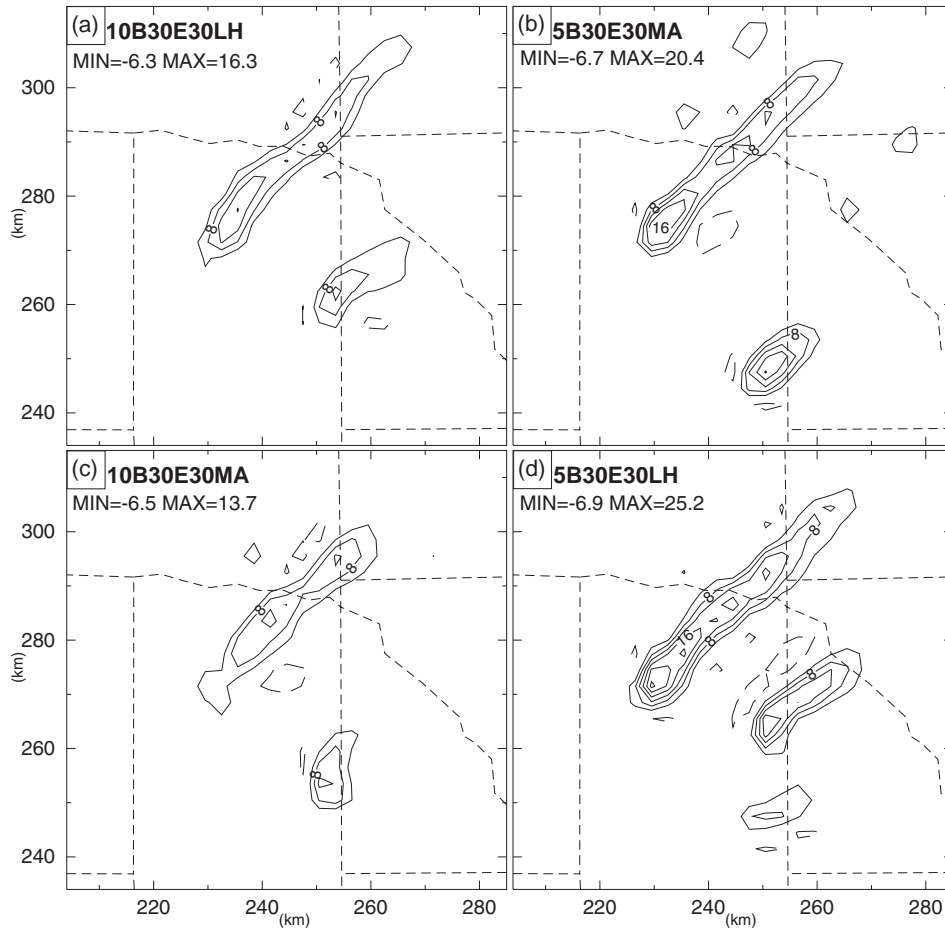


Fig. 10. The vertical velocity fields at 7 km MSL at the end of assimilation in experiments 10B30E30LH (a), 5B30E30MA (b), 10B30E30MA (c), and 5B30E30LH (d). The domain shown represents the portion of 3-km grid between 205 and 285 km in east-west direction and from 235 to 315 km in north-south direction. The contour interval is 4 ms^{-1} .

The strength and coverage of updrafts of 10B30E30LH and 5B30E30MA are between those of 10B30E30MA and 5B30E30LH. As pointed out earlier, the forecast of 10B30E30LH on the OKC storm is the best among all experiments, while the forecast of 5B30E30MA is reasonably good, although both forecasts miss the dissipation stage of the OKC storm to some degree.

The above analyses clearly show that to obtain good forecast, right combinations of the in-cloud temperature adjustment scheme and the analysis frequency are necessary, given the length of the AW. When the analysis cycles are of 10 minutes long and spans over a one hour AW, the LH scheme outperforms the MA scheme. This is however opposite when 5-minute analysis cycles are used. In this case, the MA scheme outperforms the LH scheme. Among the four experiments compared, 10B30E30LH produces the best forecast while that of 5B30E30MA is very close. Based on the analyses on the amount of potential energy added into the model by the assimilations and the response of the model atmosphere in terms of updraft strength, it is clear that the right amount of energy input is the key in promoting and sustaining observed storms, yet not over-intensifying them, leading to good forecasts over the life cycle of the storm. Since the LH scheme tends to add more energy into the system than the MA scheme, the use of LH scheme is generally preferred when analysis frequency is low

(e.g., 10 minutes), while the MA scheme is usually preferred when using e.g., 5 minute frequency. For this reason, most of the additional experiments to be examined next use the combinations of 5 minute interval and MA scheme or 10 minute interval and the LH scheme (see Table 1).

4.4. The Impact of the Length and Temporal Coverage of Assimilation Window

In the earlier experiments, the assimilations start about 10 minutes before the OKC storm initiation and cover the entire development stage of the storm. Here, ten additional experiments, classified into two groups, are conducted to study the impact of different lengths and coverage of assimilation window (AW, Table 1). For the first group of experiments, including 10B30E10, 10B30E20, 5B30E10 and 5B30E20, the assimilation starts at 2030, the same as the earlier four experiments, but ends at 2110 or 2120. The second group includes 10B40E30, 10B50E30, 10B60E30, 5B40E30, 5B50E30, and 5B60E30 and their AWs all end at 2130 but start at 2040, 2050 or 2100. Both 5 and 10-minute assimilation frequencies are tested in these two groups. For brevity, we will only show the maps of predicted reflectivity exceeding 45 dBZ at the 1.45° elevation. The results from the first group are shown in Fig. 11 and those from the second group in Fig. 12.

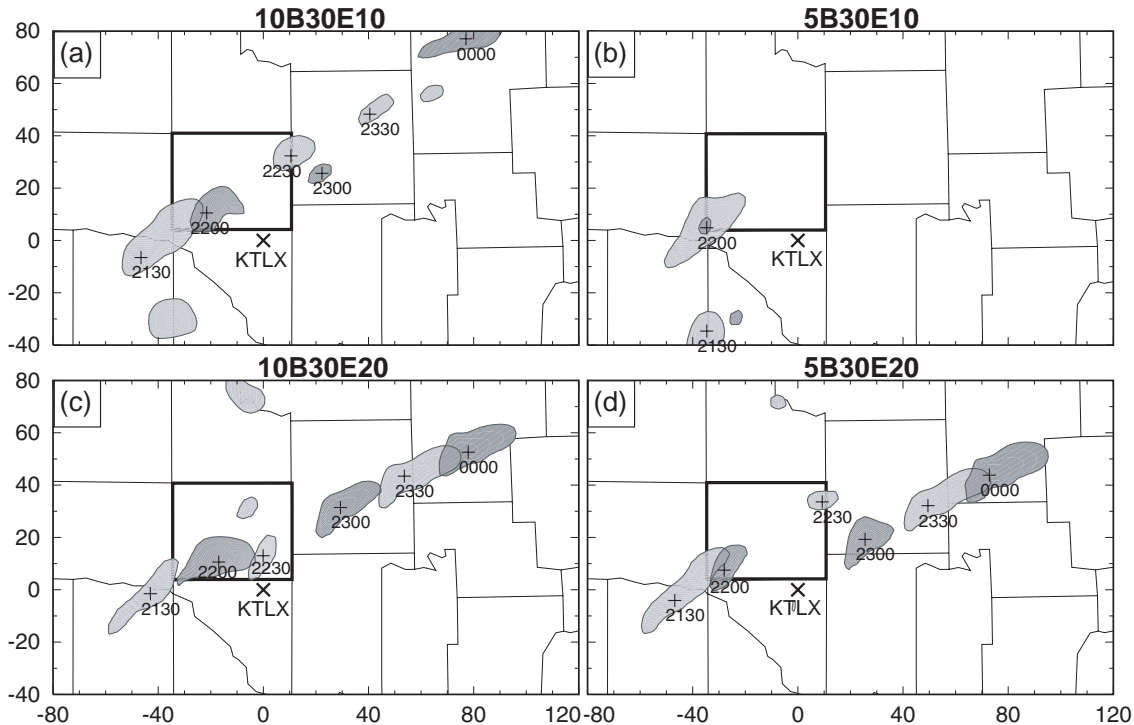


Fig. 11. As Fig. 3b, but for experiments 10B30E10 (a), 10B30E20 (c), 5B30E10 (b), and 5B30E20 (d).

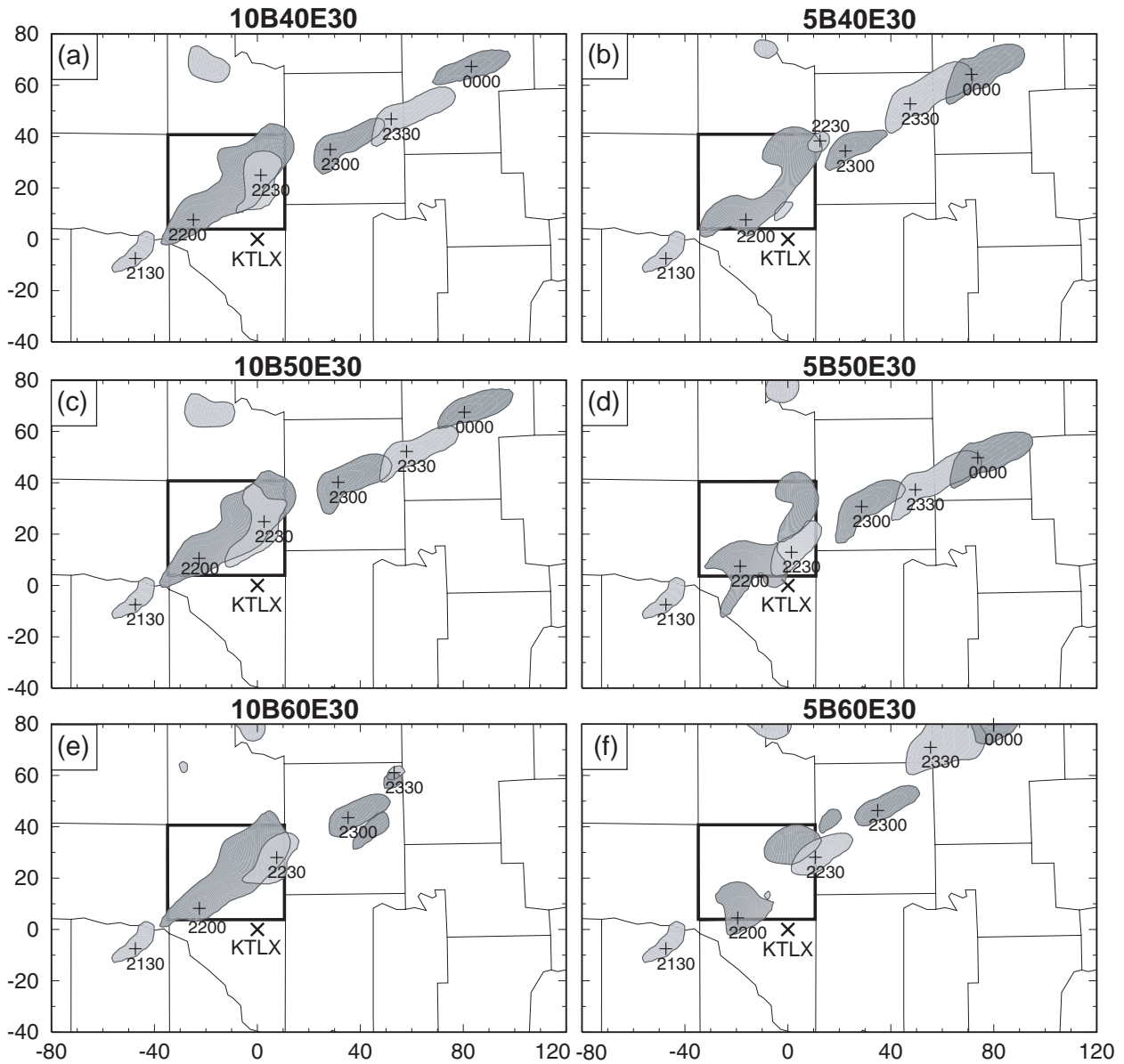


Fig. 12. As Fig. 3b, but for experiments 10B40E30 (a), 10B50E30 (c), 10B60E30 (e), 5B40E30 (b), 5B50E30 (d), and 5B60E30 (f).

As stated in the case introduction, the first echo of the OKC storm appeared at about 2040 and the echo exceeded 35 dBZ by 2101. From then on, the OKC storm grew quickly and developed into a strong supercell by 2131 (c.f., Fig. 2). The AWs of the first group of experiments mainly cover the early part of the development stage (from 2040 to 2110) of the OKC storm. In 10B30E10 and 5B30E10, the first 30 minutes of storm life (2040-2110) is covered by the 40-minute AWs (2030-2110). The predicted storm in

5B30E10 disappears completely after 2200, or 50 minutes into the forecast (Fig. 11b), while that in 10B30E10 lasts until 2230 (80 minutes into the forecast) and has correct maximum echo locations at 2130 and 2200 (Fig. 11a). A spurious cell develops in the experiment, however, southeast of the OKC storm, and is visible from 2300 on. Obviously, the OKC storm was not fully built up by the assimilation cycles and the spurious storm developing to its southeast probably had negative impact too.

When the AW is extended by 10 minutes in 10B30E20 and 5B30E20, to 2120, now including more radar observations, the forecast is improved for both. The predicted OKC storm in 5B30E20 lasts until 2230 and has better positioning at 2130 and 2200 (Fig. 11d). Similar to the 10B30E10 case, a spurious cell also develops in the model and has become stronger than the OKC storm by 2300. The OKC storm later dissipates while this spurious storm become stronger. The forecast of 10B30E20 is much better than that of 10B30E10 and appears close to the best forecast, from 10B30E30LH (Fig. 11a,c and Fig. 3b). A more detailed look at the forecast between 2200 and 2230 indicates that the predicted OKC storm actually dissipates quickly after 2200 while a new storm quickly develops in its place and propagates along the path of the observed OKC storm in the rest of the forecast. The results of this group of experiments and those from 10B30E30LH and 5B30E30MA clearly suggest that an AW of about 1-hour long, covering most of the developmental stage of the OKC storm is helpful and necessary to obtain a good analysis and subsequent forecast of the storm. At least, longer AW is helpful.

The AWs of the second group of experiments mainly cover the later development stage, from 2100 to 2130, of the OKC storm. Although the AWs from 2040 to 2130 of 10B40E30 and 5B40E30 includes all radar observations used in 10B30E30LH and 5B30E30MA, the forecasts of the former are worse than those of the latter (Fig. 12a, b, Fig. 3, Fig. 5), mainly because of larger northwestward displacement errors at the latter forecast times. These results indicate that, even though the first 10 minutes of the 3-km assimilation precede the initiation of the OKC storm therefore the availability of radar data, the additional period of AW is still beneficial. The spinning up of the 9 km solution at 2030 on the 3 km grid to arrive at a better forecast background for the 3 km analysis at 2040 must be the reason. When the AW is started even later, at 2050 or 2100, and includes only the later part of the development stage of the OKC storm, the predicted paths of OKC storm in the 10B50E30, 10B60E30, and 5B60E30 deviate northward even more (Fig. 12c, e, f), while that in 5B50E30 has correct direction but lags the observation by about 15 km at the end of forecast (Fig. 12d). There is also some discontinuous development around 2230. The results suggest that having an AW that covers the entire developmental stage as well as a pre-storm period produces the best analysis and prediction. When the AW is relatively short, covering the later part of the developing stage is

more effective in building a sustainable storm in the model.

4.5. Results of Experiment 5B60E30LH

It is found earlier that experiment 5B60E30, which uses 5 minute analysis cycles over a 30 minute AW and the MA scheme, initializes the OKC storm that dissipates quickly (Fig. 12f). Another storm that develops to the southeast of the OKC storm maintains its intensity but propagates too far north. Experiment 5B30E30LH, which uses a one hour AW with 5 minute intervals and the LH scheme, produces a storm that develops too fast (Fig. 8b), apparently due to too much potential energy added by the LH scheme. Based on these characteristics, a new experiment, 5B60E30LH, is performed, which is the same as 5B60E30 except for the LH scheme used. The question to ask is: when the assimilation window is short, can the extra potential energy afforded by the LH scheme help sustaining the initialized storm?

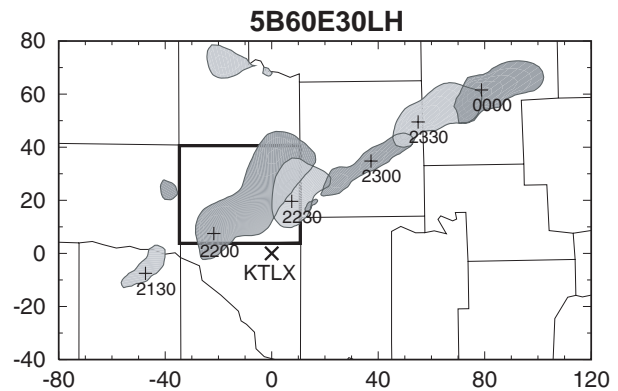


Fig. 13. As Fig. 3b, but for experiment 5B60E30LH.

The results of 5B60E30LH are shown in Fig. 13. Compared to 5B60E30, 5B30E30LH, and the observations (Fig. 13, Fig. 12f, Fig. 8b, Fig. 3a), 5B60E30LH captures the general evolution and propagation of the OKC storm rather well and the storm remains a strong supercell up to the end of the 2.5 hours of forecast. The significant improvement in the forecast of 5B60E30LH, when compared to 5B60E30, reflects the importance of a proper combination of assimilation parameters, especially when certain parameters, such as the assimilation window length, are constrained by practical limitations, such as those found with real time applications. In the case 5B60E30LH, the insufficient AW length can be compensated by using a temperature adjustment scheme that adds

more energy into the system than can otherwise be justified. In real time applications where the truth is unknown and data and computational constraints exist, careful consideration and setup of the assimilation systems are necessary, at least when using similar methods as used here.

5. FURTHER DISCUSSIONS

In this paper, the ARPS 3DVAR and cloud analysis procedures are successfully applied to the analysis and prediction of the 8 May 2003 Oklahoma City tornadic thunderstorm case, using an intermittent procedure that assimilates the scan volumes of the Oklahoma City WSR-88D Doppler radar (KTLX) with proper assimilation configurations.

A 3-km grid nested within a 9-km grid is used for both assimilation and forecast. The 3DVAR is used to analyze conventional observations and the radial velocity data, in a similar way as used in Hu et al. (2005b). The cloud analysis is performed on the 3-km grid to analyze the reflectivity data and to build up the model storm through intermittent assimilation cycles. Forecasts for up to 2.5 hours are performed starting from the assimilated initial conditions, and their quality is used to evaluate the performance of assimilation.

A total of fifteen 3-km experiments with different assimilation configurations are conducted to study the impact of the analysis frequency, in-cloud temperature adjustment scheme, and the length and coverage of the assimilation window on the final analysis and forecast.

The best forecast for the OKC storm comes from the experiment that uses a one-hour long assimilation window with 10-minute analysis cycles and an in-cloud temperature adjustment scheme that is based on latent heat released related to the input of cloud condensate, or the LH scheme. The experiment accurately predicts the propagation of the OKC storm with position errors of less than 8 km throughout the 2.5 hours of forecast, in terms of the maximum reflectivity. The supercell characteristics of the storm during the forecast are also well captured even though the grid space of the experiment is a relatively coarse 3 km for the purpose of resolving the tornado vortex or even the mesocyclone. The predicted middle and low-level vorticity fields show a strong vorticity maxima column associated with the predicted OKC storm during the entire forecast (not shown).

It is interesting to note here that a preliminary study by Wicker and Dowell (2004) performed an assimilation and prediction study on this same

case. The theoretically more advanced ensemble Kalman filter (EnKF) method is used, using a 1-km horizontal resolution and assimilating six scan volumes of an experimental WSR-88D radar (KOUN) located in Norman, Oklahoma. The assimilation spans over nearly 40 minutes. The radar reflectivity field at the end of assimilation looks very close to the observed one, and the wind fields appear dynamically consistent too, and probably more so than the analyzed fields in our experiments. Unfortunately, the predicted storm in the case does not last beyond 40 minutes. Apart from the assimilation methods used, another significant difference between our and their studies lies in the fact that a single sounding is used to define the storm environment in their case - the representativeness of this time-invariant environment may be a cause of the less successful prediction. Further, our experiments employ a full physics package rather than cloud physics only.

When the higher assimilation frequency, i.e., a 5-minute time interval, is used with one-hour AW and moist-adiabat (MA) scheme (in 5B30E30MA), the quality of the forecast is worse than the corresponding experiment (10B30E30LH) with 10 minute intervals, even though more radar observations are assimilated in the former. This behavior is related to the capabilities of our analysis scheme. The correlation among different analysis variables or the balance among them is not considered in either the ARPS 3DVAR or cloud analysis, even though the latter employs a cloud physics model to determine the cloud and hydrometeor contents. Starting from such initial conditions that are not in balance with the prediction model, significant adjustment occurs within the initial period of prediction. This is clearly seen from the time series of maximum vertical velocity. It is found that the model almost always requires more than 5 minutes to complete the initial adjustments and a 10 minute analysis interval is needed to give the model enough time to establish balance among the model fields and to build a sustainable storm. When more advanced analysis methods that can produce well balanced analysis fields, such as the ensemble Kalman filter or 4DVAR methods, are used, the more data are assimilated, the better should be the final analysis. This is shown to be true in Xue et al. (2005) through OSSEs (Observing System Simulation Experiments) that the assimilation of 1-minute volume scans produces better results than volume scans taken at lower frequencies, for a supercell storm.

The impact of two in-cloud temperature adjustment schemes available in the ARPS cloud analysis procedure is also studied. The experiments show that the assimilation (5B30E30LH) using the latent heating-based (LH) scheme at 5 minute intervals over a 1-hour AW adds too much potential energy into the storm system, which causes a too fast development of the main storm and the triggering and intensification of a spurious cell. On the other hand, the assimilation using MA scheme with 10 minute intervals over the same length of AW adds too little potential energy instead, which delays the development of the main storm during the assimilation and forecast. A combination of 10 minute analysis intervals with the LH scheme or 5 minute intervals with the MA scheme is found to work the best for one hour long assimilation windows.

The experiments testing the impact of the lengths and coverage of AW are also interesting. It is found that taking only 10 minutes out of the one-hour long assimilation window either at the beginning or the end can significantly reduce the forecast quality of the main storm, and in general the shorter the AW, the worse the forecast. In practice, it is desirable to use an assimilation window that is as short as possible, in order to have an as-long-as-possible forecast lead time, and in this case a long lead time for forecasting the tornado outbreak. Our experiments indicate that an AW of at least 30 minutes is necessary. In our 28 March 2000 downtown Fort Worth tornadic thunderstorm case (Hu *et al.* 2005a; Hu *et al.* 2005b), a lead time of over one hour is achieved for the prediction of strong low-level rotation that appears to be closely linked to the observed tornadogenesis, and a similar assimilation system as used here was used with one hour long window and 10 minute analysis intervals, and the MA scheme.

To see what we can do with a 30 minute assimilation window located at the later stage of the storm development, experiment 5B60E30 which produces too weak a OKC storm that dissipates quickly, is repeated using the LH scheme in 5B60E30LH. As expected, the extra heating added by the LH scheme accelerates the development of the main storm. The forecast of the OKC storm is rather good. Compared to 10B30E30LH, the shortened AW is compensated by about twice as many analysis cycles. Since the LH scheme has the tendency to add an amount of heating that is somewhat independent of the background state, the total amount of heating added tends to be proportional to the number of

analysis cycles. Such results are also consistent with the analysis on the temperature adjustment by Hu *et al.* (2005b).

The above conclusions are mainly based on the 8 May 2003 Oklahoma City tornadic storm case, although some suggests have also been drawn from our earlier study on the Fort Worth tornadic thunderstorm case. The quantitative aspects may also be tied to the specific analysis schemes used, i.e., the ARPS 3DVAR and cloud analysis. A general conclusion is that the assimilation configurations can significantly impact the results of radar data assimilation and subsequent storm forecast. The configurations should be carefully evaluated and tested, in a similar but perhaps even more thorough way than is done here. When continuous assimilation cycles are used, at, say, 5 minutes intervals, the optimal assimilation window length is still an issue for a given scheme. The experiments on AW coverage provide us with some guidance on the design of post-real-time assimilation experiments, and for real time applications provide some guidance on the results we can expect.

Even though theoretically less than optimal, the current intermittent assimilation procedure for incorporating full-volume Doppler radar data into a storm prediction model is computationally inexpensive and operationally feasible. For real time operational applications, the computation efficiency of a configuration may carry more weight. When similar forecast qualities are obtained, an assimilation configuration that requires that least amount of data processing and computation, and provides the longest forecast lead time for the features that we are most interested is obviously preferred, and such a configuration may be the one of choice even if the resultant prediction is slightly worse. Future, similar issues for other types of convective systems, such as the less persistent multi-cellular storms and the larger scale squall line and MCSs (mesoscale convective systems) should also be investigated.

6. SUMMARY

Finally, we briefly summarize the key results of this study as follows.

- 1) The ARPS 3DVAR and cloud analysis procedure are applied to the 8 May 2003 Oklahoma City tornadic thunderstorm case in a cycled mode on a 3-km grid. Volume scans of data from the OKC WSR-88D radar are assimilated.

- 2) Successful predictions are obtained by using several different combinations of analysis cycle interval, assimilation window (AW) length and in-cloud temperature adjustment scheme. Experiments with 10 minute interval, 1 hour AW, and LH adjustment scheme (10B30E30LH), with 5 minute interval, 1 hour AW, and MA scheme (5B30E30MA), and with 5 minute interval, 30 minute AW, and the LH scheme (5B60E30LH) all produce reasonable forecasts for up to 2.5 hours, with the forecast of 10B30E30LH being the best.
- 3) The configuration of 5B30E30MA is theoretically the best, because all radar scan volumes within an assimilation window that covers the entire development period of the main storm are used, together with a temperature adjustment scheme that is based on a simple cloud physics model and is less sensitive to the number of cycles applied because it makes only the adjustment necessary to fit a diluted moist adiabat (Brewster 2002; Hu *et al.* 2005b).
- 4) The configuration used by 5B60E30LH has a shorter AW therefore has a lower computational cost. The reduced AW length is compensated by the extra potential energy input provided by the LH scheme, resulting in a reasonably well developed storm by the end of AW.
- 5) Due to significant adjustment in the forecast following each analysis, shorter assimilation cycles does not necessarily produce better final analysis. Ten minutes cycles that assimilate every other scan volumes are found to work better.
- 6) A short spin-up period (~10 minutes) on the high resolution grid before any radar data are available is found to be beneficial.
- 7) When the AW length is limited, to e.g., 30 minutes, an AW at the later part of the development stage of storm is more effective than that applied at the early part, although difference in the actual time of forecast initial condition may have also played a role.

Acknowledgments. This work was mainly supported by NSF grant ATM-0129892 and a DOT-FAA grant via DOC-NOAA NA17RJ1227. Xue was also supported by NSF grants ATM-0331756, ATM-0331594, EEC-0313747, and by "Outstanding Overseas Scholars" awards from Chinese Natural Science Foundation (No. 40028504) and from Chinese Academy of Sciences (No. 2004-2-7). Drs. Keith Brewster and Jidong Gao are thanked for very helpful

discussions. Supercomputers at Pittsburgh Supercomputing Center were used for most of the experiments.

REFERENCES

- Bratseth, A. M., 1986: Statistical interpolation by means of successive corrections. *Tellus*, 38A, 439-447.
- Brewster, K., 1996: Application of a Bratseth analysis scheme including Doppler radar data. *Preprints, 15th Conf. Wea. Anal. Forecasting*, Norfolk, VA, Amer. Meteor. Soc., 92-95.
- , 2002: Recent advances in the diabatic initialization of a non-hydrostatic numerical model. *Preprints, 15th Conf on Numerical Weather Prediction and 21st Conf on Severe Local Storms*, San Antonio, TX, Amer. Meteor. Soc., J6.3.
- Crum, T. D. and R. L. Alberty, 1993: The WSR-88D and the WSR-88D operational support facility. *Bull. Amer. Meteor. Soc.*, 74, 1669-1687.
- Gal-Chen, T., 1978: A method for the initialization of the anelastic equations: Implications for matching models with observations. *Mon. Wea. Rev.*, 106, 587-606.
- Gao, J., M. Xue, K. Brewster, F. Carr, and K. K. Droegemeier, 2002: New Development of a 3DVAR system for a nonhydrostatic NWP model. *Preprint, 15th Conf. Num. Wea. Pred. and 19th Conf. Wea. Anal. Forecasting*, San Antonio, TX, Amer. Meteor. Soc., 339-341.
- Gao, J.-D., M. Xue, K. Brewster, and K. K. Droegemeier, 2004: A three-dimensional variational data analysis method with recursive filter for Doppler radars. *J. Atmos. Ocean. Tech.*, 21, 457-469.
- Gao, J.-D., M. Xue, A. Shapiro, Q. Xu, and K. K. Droegemeier, 2001: Three-dimensional simple adjoint velocity retrievals from single Doppler radar. *J. Atmos. Ocean Tech.*, 18, 26-38.
- Hu, M., M. Xue, and K. Brewster, 2005a: 3DVAR and Cloud analysis with WSR-88D Level-II Data for the Prediction of Fort Worth Tornadic Thunderstorms. Part II: Impact of radial velocity analysis via 3DVAR. *Mon. Wea. Rev.*, Conditionally accepted.
- Hu, M., M. Xue, J. Gao, and K. Brewster, 2005b: 3DVAR and Cloud analysis with WSR-88D Level-II Data for the Prediction of Fort Worth Tornadic Thunderstorms. Part I: Cloud analysis and its impact. *Mon. Wea. Rev.*, Conditionally accepted.
- Qiu, C. and Q. Xu, 1994: A spectral simple adjoint method for retrieving low-altitude winds from

- single-Doppler data. *J. Atmos. Oceanic Technology*, 11, 927-936.
- Qiu, C.-J. and Q. Xu, 1992: A simple adjoint method of wind analysis for single-Doppler data. *J. Atmos. Oceanic Technol.*, 9, 588-598.
- Schaefer, J. T., 1990: The critical success index as an indicator of warning skill. *Wea. Forecasting*, 5, 570-575.
- Serafin, R. J. and J. W. Wilson, 2000: Operational Weather Radar in the United States: Progress and Opportunity. *Bulletin of the American Meteorological Society*, 81, 501-518.
- Shapiro, A., S. Ellis, and J. Shaw, 1995: Single-Doppler radar retrievals with Phoenix II data: Clear air and microburst wind retrievals in the planetary boundary layer. *J. Atmos. Sci.*, 52, 1265-1287.
- Snyder, C. and F. Zhang, 2003: Assimilation of simulated Doppler radar observations with an ensemble Kalman filter. *Mon. Wea. Rev.*, 131, 1663-1677.
- Sun, J. and N. A. Crook, 1997: Dynamical and microphysical retrieval from Doppler radar observations using a cloud model and its adjoint. Part I: Model development and simulated data experiments. *J. Atmos. Sci.*, 54, 1642-1661.
- , 1998: Dynamical and Microphysical Retrieval from Doppler Radar Observations Using a Cloud Model and Its Adjoint. Part II: Retrieval Experiments of an Observed Florida Convective Storm. *J. Atmos. Sci.*, 55, 835-852.
- Sun, J., D. W. Flicker, and D. K. Lilly, 1991: Recovery of three-dimensional wind and temperature fields from simulated single-Doppler radar data. *J. Atmos. Sci.*, 48, 876-890.
- Tong, M. and M. Xue, 2005: Ensemble Kalman filter assimilation of Doppler radar data with a compressible nonhydrostatic model: OSS Experiments. *Mon. Wea. Rev.*, In press.
- Weygandt, S. S., A. Shapiro, and K. K. Droegemeier, 2002a: Retrieval of Model Initial Fields from Single-Doppler Observations of a Supercell Thunderstorm. Part I: Single-Doppler Velocity Retrieval. *Mon. Wea. Rev.*, 130, 433-453.
- , 2002b: Retrieval of Model Initial Fields from Single-Doppler Observations of a Supercell Thunderstorm. Part II: Thermodynamic Retrieval and Numerical Prediction. *Mon. Wea. Rev.*, 130, 454-476.
- Wicker, L. J. and D. C. Dowell, 2004: High-resolution analyses of the 8 May 2003 Oklahoma City storm. Part III: An ultra-high resolution forecast experiment. *Preprints, 22nd Conf. Severe Local Storms., Hyannis, MA, Amer. Meteor. Soc., CDROM*, 12.6.
- Xu, Q., C. Qiu, and J. Yu, 1994: Adjoint-method retrievals of low-altitude wind fields from single-Doppler reflectivity measured during Phoenix II. *J. Atmos. Oceanic Technology*, 11, 275-288.
- Xue, M., K. K. Droegemeier, and V. Wong, 2000: The Advanced Regional Prediction System (ARPS) - A multiscale nonhydrostatic atmospheric simulation and prediction tool. Part I: Model dynamics and verification. *Meteor. Atmos. Physics*, 75, 161-193.
- Xue, M., M. Tong, and K. K. Droegemeier, 2005: An OSSE framework based on the ensemble square-root Kalman filter for evaluating impact of data from radar networks on thunderstorm analysis and forecast. *J. Atmos. Ocean Tech.*, Under review.
- Xue, M., K. K. Droegemeier, V. Wong, A. Shapiro, and K. Brewster, 1995: ARPS Version 4.0 User's Guide. [Available at <http://www.caps.ou.edu/ARPS>], 380 pp.
- Xue, M., K. K. Droegemeier, V. Wong, A. Shapiro, K. Brewster, F. Carr, D. Weber, Y. Liu, and D. Wang, 2001: The Advanced Regional Prediction System (ARPS) - A multi-scale nonhydrostatic atmospheric simulation and prediction tool. Part II: Model physics and applications. *Meteor. Atmos. Phys.*, 76, 143-166.
- Zhang, F., C. Snyder, and J. Sun, 2004: Impacts of initial estimate and observations on the convective-scale data assimilation with an ensemble Kalman filter. *Mon. Wea. Rev.*, 132, 1238-1253.
- Zhang, J., 1999: Moisture and Diabatic Initialization Based on Radar and Satellite Observation, School of Meteorology, University of Oklahoma, 194.
- Zhang, J., F. Carr, and K. Brewster, 1998: ADAS cloud analysis. *Preprints, 12th Conf. on Num. Wea. Pred., Phoenix, AZ., Amer. Met. Soc.*, 185-188.